Thesis Progression Report

Anatole Verhaegen

July 10, 2015

Contents

Nomenclature

ρ_m linear mass density

$\rho_{m_{booster}}$ linear mass density of the booster

$\rho_{m_{dart}}$ linear mass density of the dart

E_i Young modulus of beam i

F_i external force along z-axis applied on node i

G center of gravity

$I_{G,y,i}$ or I_i second moment of area of beam i

$I_{G,y_{booster}}$ second moment of area of the booster about the neutral axis along the y-axis

$I_{G,y_{dart}}$ second moment of area of the dart about the neutral axis along the y-axis

$I_{G,y}$ second moment of area about the neutral axis along the y-axis

L missile length

l length of an element beam

m missile mass

m_i mass of node i

$M_{y,i}$ external moment along y-axis applied on node i

n number of nodes

E   longitudinal Young modulus of the missile

Part I
Modeling

1   Characteristics

2   Flight Dynamics

2.1   Mass Properties

ASTER-30 has two parts. The booster weights $m_{booster} = 310\,kg$ and will lose mass along the acceleration phase. However, it is considered that its mass is constant at 310kg to simplify the model. The dart weights $m_{dart} = 140\,kg$ during the complete flight. The total mass of the missile is then $m = 450\,kg$ With no more information on mass distribution, it is assumed that the mass is uniformly distributed in the booster and in the dart. The length of the booster is $L_{booster} = 2.2m$ and the dart is lightly longer with $L_{dart} = 2.7m$

The center of gravity G position is at $x_{CG} = \frac{\int x\,dm}{m}$. With the assumption on mass distribution,

$$x_{CG} = \frac{\frac{1}{2}L_{booster}\,m_{booster} + (L_{booster} + \frac{1}{2}L_{dart})\,m_{dart}}{m}$$

that yields $x_{CG} = 1.86\,m$.

The rotational inertia at the center of gravity and about the y-axis is $J_y = \int (x - x_{CG})^2 dm$ giving

$$J_y = \frac{1}{3}\frac{m_{booster}}{L_{booster}}\left[(L_{booster} - x_{CG})^3 + x_{CG}^3\right] + \frac{1}{3}\frac{m_{dart}}{L_{dart}}\left[(L_{dart} + L_{booster} - x_{CG})^3 - (L_{booster} - x_{CG})^3\right]$$

Finally $J_y = 789\,kg.m^2$.

2.2   Aerodynamics

An aerodynamic model is needed to derive the equations of motion. The atmosphere and the variation of air density will first be defined, then the main body aerodynamics will be described ending with the fins aerodynamics.
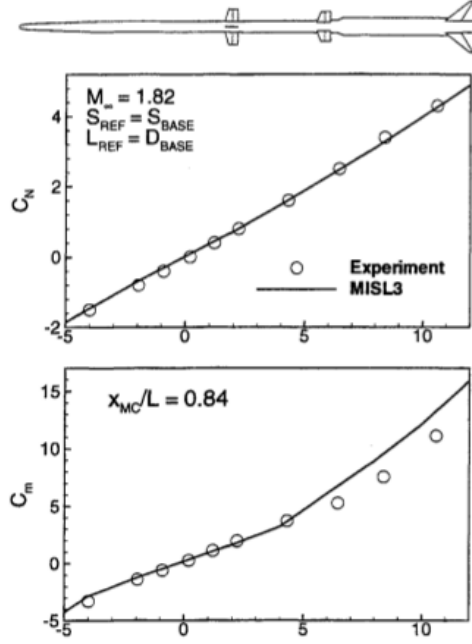
Figure 1: Flared Missile Lift and Pitching Moment Coefficients [4]

2.2.1   Standard Atmosphere

For the atmosphere model, the International Standard Atmosphere is considered.

2.2.2   Main Body Aerodynamics

The reference surface for this kind of airframe is the cross-section of the missile. The bigger cross-section is at the booster and will be taken as reference surface. Thus $S_{ref} = \pi D^2_{booster}/4$. The length reference will be the largest diameter $L_{ref} = D_{booster}$.

ASTER-30 has a body which is very similar to the flared frame studied in [4]. Some of its aerodynamic data are in Figure 1. In this figure, the x-axis is oriented from nose to tail contrary to this thesis.

The lift coefficient slope in this paper is $C_{L\alpha} = 22\,rad^{-1}$. Since the airframe is symmetric about its xy-plane, $C_{L0} = 0$. Similarly, the zero angle of attack pitching moment coefficient $C_{m0} = 0$. In this paper, the pitching moment coefficient slope is $C_{m\alpha} = 45\,rad^{-1}$ at $x_{CM} = 0.78\,m$. However, this coefficient would place the aerodynamic center at $x_{AC} = \frac{L_{ref}C_{m\alpha}}{C_{L\alpha}} + x_{CM} = 1.52\,m$. This aerodynamic center in this paper is too aft for this airframe compared to the center of gravity at $x_{CG} = 1.86\,m$. The aerodynamic center will be placed $7\,cm$ aft of the center of gravity at $x_{AC} = 1.79\,m$. This yields a pitching moment coefficient slope of $C_{m\alpha} = -4.3\,rad^{-1}$ **at the center of gravity**.

The drag coefficient for such a missile is given in [2]. The zero-lift drag is $C_{D0} = 0.95$ and the drag slope is estimated to be $k_D = 1$.

2.2.3   Fins Aerodynamics

2.3   External Efforts

Several external forces act on the missile airframe. These forces are due to gravity, aerodynamics and propulsion. It is important to describe clearly the frames in which they are defined.

2.3.1   Frames

There are four frames to define. They all have the axis $\vec{y_0} = \vec{y}$ in common because the dynamics considered are only in the xz-plane.

The first one is the Earth's frame $(\vec{z_0}, \vec{x_0})$ where $\vec{z_0}$ is vertical and oriented downward. $\vec{x_0}$ is oriented forward.

The second one is the aerodynamic frame $(\vec{z_a}, \vec{x_a})$ with $\vec{x_a}$ along the speed vector of the missile and $\vec{z_a}$ normal to $\vec{x_a}$ and oriented downward. The flight path frame is obtained by rotating the Earth's frame of an angle of γ the flight path angle around $\vec{y}$.

The third one is the body frame $(\vec{z_b},\vec{x_b})$ where $\vec{x_b}$ is along the body axis and $\vec{z_b}$ normal to $\vec{x_b}$ and oriented downward. The body frame is obtained by rotating the Earth's frame of an angle of α the angle of attack around $\vec{y}$. The pitch angle is $\theta = \alpha + \gamma$.

The last one is the propulsion frame $(\vec{z_T},\vec{x_T})$ where $\vec{x_T}$ is along the thrust vector and $\vec{z_T}$ is normal to it and oriented downward. This last frame is obtained by rotating the body frame by an angle of θ_T - the nozzle angle - around $\vec{y}$.

2.3.2   Gravity

The gravity is assumed to be uniform during the flight and equal to the standard gravity value $g = 9.81 \, m.s^{-2}$. Gravity is creating a force called weight applied at the center of gravity of the airframe and acting along the z-axis. This force is denoted $\vec{W}$ and

$$\vec{W} = m \, g \, \vec{z_0}$$

2.3.3   Aerodynamic Efforts

The aerodynamic efforts can be divided into a lift force, a drag force and a pitching moment. The moment created by the lift and the drag is gathered into the pitching moment at the center of gravity.

Lift   The lift is acting normal to the flight path along $\vec{z_a}$ of amplitude L:

$$L = \frac{1}{2}\rho S_{ref} V^2 C_L$$

where $C_L = C_{L0} + C_{L\alpha}\alpha$.

Drag   The drag is acting along the flight path $\vec{x_a}$ and oriented opposite to the speed vector and of amplitude D.

$$D = \frac{1}{2}\rho S_{ref}V^2 C_D$$

with $C_D = C_{D0} + k_D C_L^2$.

Pitching Moment   The pitching moment at the center of gravity is acting along the y-axis with an amplitude of M:

$$M = \frac{1}{2}\rho S_{ref}V^2 D_{ref}C_m$$

with $C_m = C_{m0} + C_{m\alpha}\alpha$.

2.3.4   Propulsion Efforts

The thrust is oriented along $\vec{x_T}$ thanks to the orientable nozzle. The propulsion force is then

$$\vec{T} = T\vec{x_T}$$

2.4   Equations of Motion

The Equations of Motion are projected in the aerodynamic frame $(\vec{z_a}, \vec{x_a}, \vec{y})$. This gives three equations: the propulsion equation, the lift equation and the pitching moment equation.

2.4.1   Linear Acceleration

The linear acceleration of the center of gravity in an inertial frame of reference is linked to the sum of external forces by the mass of the airframe:

$$m\,\vec{a}_{CG/\mathcal{R}_e} = \sum \vec{F}_{external} \tag{1}$$

The acceleration in $\mathcal{R}_e$ is

$$\vec{a}_{CG/\mathcal{R}_e} = \left[\frac{d\vec{V}}{dt}\right]_{\mathcal{R}_e}$$

The speed vector $\vec{V}$ must be differentiated in the aerodynamic frame which is not an inertial frame of reference to link the acceleration with the aerodynamic parameters. The vector $\vec{V}$ differentiated in the moving frame $\mathcal{R}_a$ relative to the frame $\mathcal{R}_e$ follows the following formula:

$$\left[\frac{d\vec{V}}{dt}\right]_{\mathcal{R}_e} = \left[\frac{d\vec{V}}{dt}\right]_{\mathcal{R}_a} + \vec{\Omega}_{\mathcal{R}_a/\mathcal{R}_e} \wedge \vec{V}$$

thus

$$\left[\frac{d\vec{V}}{dt}\right]_{\mathcal{R}_e} = \dot{V}\,\vec{x_a} - \dot{\gamma}\,V\,\vec{z_a}$$

Equation 1 is then projected in the aerodynamic frame $(\vec{z_a}, \vec{x_a})$:

$$\begin{cases} m\,\dot{V} &= \sum \vec{F}_{external} \cdot \vec{x_a} \\ -m\,V\,\dot{\gamma} &= \sum \vec{F}_{external} \cdot \vec{z_a} \end{cases}$$

Finally, developping the sum of forces the first equation gives the propulsion equation:

$$m\,\dot{V} = -D + T\,\cos(\theta_T + \alpha) - W\,\sin(\gamma) \tag{2}$$

The second equation gives the lift equation:

$$-m\,V\,\dot{\gamma} = -L - T\,\sin(\theta_T + \alpha) + W\,\cos(\gamma) \tag{3}$$

2.4.2   Pitching Moment Equation

The pitching moment equation at the center of gravity along the y-axis is

$$J_y\,\dot{q} = \sum \vec{M}_{external}$$

Thus developping the pitching moment yields

$$J_y\,\dot{q} = M - T\,\sin(\theta_T)\,x_{CG} \tag{4}$$

2.5   Trim

At the trim state, the altitude is constant so $\gamma = \gamma_0 = 0\,rad$.

The speed of the missile is chosen to be Mach 2 at sea level and standard temperature, hence $V = V_0 = M\,a$. The speed of sound is

$$a = \sqrt{\gamma r T} = \sqrt{1.4 \cdot 287 \cdot (273.15 + 15)} = 340\,m.s^{-1}$$

Thus $V_0 = 680\,m.s^{-1}(= 1322\,kts)$.

The acceleration of the missile is said to be about 15g which corresponds to $\dot{V}_0 = 147\,m.s^{-2}$.

The altitude is said to be sea level then $\rho_0 = 1.21\,kg.m^{-3}$.

The other derivatives $\dot{\gamma}_0$, $\dot{q}_0$, q_0 are zero.

Using the relation $\theta = \alpha + \gamma$, the Equations 2, 3 and 4 only unknowns at trim state are α_0, T_0 and θ_{T0}. The solving of this system of equation gives the following result:

$$\begin{cases} \alpha_0 & = 0.030\,rad = 1.7° \\ T_0 & = 71.3\,kN \\ \theta_{T0} & = -1.3 \cdot 10^{-3}\,rad = 0.072° \end{cases}$$

2.6 State Space System

The state vector considered for the state-space model is

$$x = \begin{bmatrix} \bar{\alpha} \\ q \end{bmatrix}$$

where q is the pitch rate and $\bar{\alpha}$ is the deviation of α from the trim value α_0:

$$\bar{\alpha} = \alpha - \alpha_0$$

The state vector is only of dimension 2 because it is assumed that all the other variables like γ , $\dot{\gamma}$, V or ρ have a very slow dynamic. Indeed in study is interested about lateral acceleration generation, which happens faster than a change of navigation variables such as γ or V.

The input vector here is $u = \bar{\theta}_T$ which is the only parameter that the controller commands. $\bar{\theta}_T$ is the deviation of θ_T from θ_{T0}.

The output vector is

$$y = \begin{bmatrix} q \\ a_{z_a CG} \\ a_{\bar{z_b}10} \\ a_{\bar{z_b}54} \\ a_{\bar{z_b}83} \\ a_{\bar{z_b}92} \end{bmatrix}$$

where $a_{z_a CG}$ is the inertial acceleration normal to the speed vector at the center of gravity, is the inertial acceleration normal to the body at node i and $a_{\bar{z_b}i}$ is the deviation of $a_{z_b i}$ from the trim value $a_{z_b i0}$. Indeed, $a_{z_b i0}$ is not zero at all. The missile is in constant acceleration at about 15g and has a trim angle of attack of $\alpha_0 = 0.030\,rad$, thus $a_{z_b i0} = 15 \cdot 0.030 = 0.45g$. Moreover $a_{z_b i}$ will vary with a change in angle of attack because of the forward acceleration projected normaly to the body. The missile onboard computer is probably able to substract this component on the lateral acceleration. To simplify this problem that is not the purpose of the study, it will be assumed that $a_{\bar{z_b}i} = a_{z_a i}$. This means that an accelerometer fixed on the body is assumed to measure only the inertial acceleration normal to the speed vector. $a_{z_a i}$ will now be simply denoted a_{zi}. Thus

$$y = \begin{bmatrix} q \\ a_{zCG} \\ a_{z10} \\ a_{z54} \\ a_{z83} \\ a_{z92} \end{bmatrix}$$

The nodes are defined in Subsection 3.1 on page 11. The pitch rate q and acceleration a_{z83} are measured to control the rigid-body states of the missile. These measurements are already integrated in the current version of ASTER-30. The acceleration measurements at nodes 10, 54 and 92 will be used to measure the vibrations due to bending oscillations. The vibration components of these accelerations will be added later. The lateral acceleration of the center of gravity is measured to assess the system. Indeed, the controller will make this output equal to the reference acceleration.

2.6.1   State Equation

The two equations that governs the dynamic of this state-space system are Equations 3 and 4. Equation 3 can be rearrange using $\dot{\gamma} = q - \dot{\alpha}$ to give

$$\dot{\alpha} = \frac{1}{mV} \left(-\frac{1}{2}\rho S_{ref}V^2(C_{L0} + C_{L\alpha}\alpha) - T\,\sin(\theta_T + \alpha) + W\,\cos(\gamma) \right) + q \qquad (5)$$

Equation 4 yields

$$\dot{q} = \frac{1}{J_y} \left(\frac{1}{2}\rho S_{ref}V^2 L_{ref}(C_{m0} + C_{m\alpha}\alpha) - T\,\sin(\theta_T)\,x_{CG} \right) \qquad (6)$$

The linearization of the two last Equations 5 and 6 about the trim state where $[\alpha, V, \rho, \theta_T, T, \gamma] = [\alpha_0, V_0, \rho_0, \theta_{T0}, T_0, \gamma_0]$. This bring the following matrix equation:

$$\begin{bmatrix} \dot{\bar{\alpha}} \\ \dot{q} \end{bmatrix} = A \begin{bmatrix} \bar{\alpha} \\ q \end{bmatrix} + B\,\bar{\theta}_T$$

where

$$A = \begin{bmatrix} A_{11} & A_{12} \\ A_{21} & A_{22} \end{bmatrix}$$

$$\begin{cases} A_{11} & = -\frac{1}{mV_0}\left(\frac{1}{2}\rho_0 S_{ref}V_0^2 C_{L\alpha} + T_0\,\cos(\theta_{T0} + \alpha_0)\right) \\ A_{12} & = 1 \\ A_{21} & = \frac{1}{J_y}\frac{1}{2}\rho_0 S_{ref}V_0^2 L_{ref}C_{m\alpha} \\ A_{22} & = 0 \end{cases}$$

and

$$B = \begin{bmatrix} -\frac{T_0 \, \cos(\theta_{T0}+\alpha_0)}{m \, V_0} \\ -\frac{T_0 \, \cos(\theta_{T0}) \, x_{CG}}{J_y} \end{bmatrix}$$

A numerical computation gives the following results:

$$A = \begin{bmatrix} -0.498 & 1 \\ -7.22 & 0 \end{bmatrix}, \quad B = \begin{bmatrix} -0.233 \\ -168 \end{bmatrix}$$

2.6.2   Output Equation

The pitch rate q is already a state so adding this signal to the output is done easily.

The inertial acceleration a_{zCG} is normal to the speed vector and has been derived in Subsection 2.4.1 on page 6:

$$a_{zCG} = \frac{1}{m} \left(-L - T \, \sin(\theta_T + \alpha) + W \, \cos(\gamma) \right)$$

Thus when linearized

$$a_{zCG} = -\frac{1}{m} \left(\frac{1}{2} \rho_0 S_{ref} V_0^2 C_{L\alpha} + T_0 \, \cos(\theta_{T0} + \alpha_0) \right) \alpha - \frac{T_0 \, \cos(\theta_{T0} + \alpha_0)}{m} \bar{\theta}_T$$

Given x the abscissa of a point on the missile, the lateral acceleration measured at this point will be

$$a_{z,x} = a_{z,CG} + (x_{CG} - x)\dot{q}$$

Hence using Equation 4 and linearizing

$$a_{z,x} = a_{z,CG} + \frac{1}{J_y}(x_{CG} - x) \left(\frac{1}{2} \rho_0 S_{ref} V_0^2 L_{ref} C_{m\alpha} \alpha - T_0 \, \cos(\theta_{T0}) \, x_{CG} \, \bar{\theta}_T \right)$$

For a node i, $x_i = (i - 1) \, l$.
This yields the output equation

$$y = C \begin{bmatrix} \bar{\alpha} \\ q \end{bmatrix} + D\bar{\theta}_T$$

The matrices C and D will only be given numerically:

$$C = \begin{bmatrix} 0 & 1 \\ & \\ & \\ & \end{bmatrix} \quad D = \begin{bmatrix} \\ \\ \\ \end{bmatrix}$$
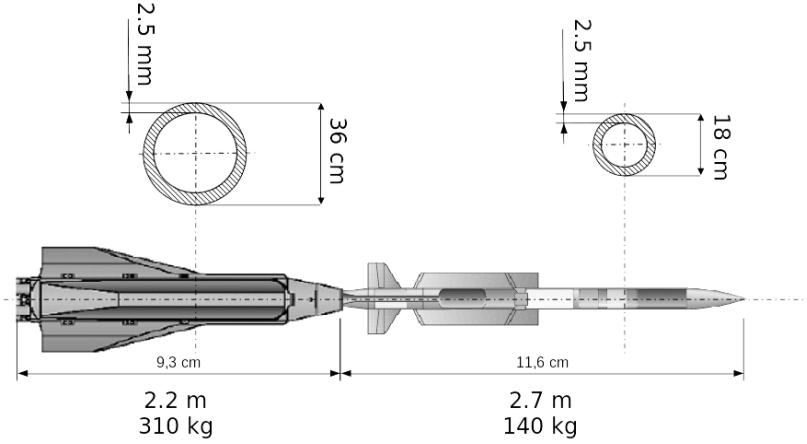
Figure 2: ASTER-30 Dimensions

3 Structural Model

3.1 From continuous to discrete

ASTER-30 length is 4.9 m and the largest diameter is 0.36 m on the booster so the missile can be considered as a beam with variable cross section. Euler-Bernoulli beam theory is suitable here because higher order models like Timoshenko beam theory would bring additive complexity and precision that are not needed for this study. Therefore sections rotational inertia and shear deformation are neglected. For the purpose of this study, only bending along y-axis is considered so deformations of the missile are contained in the zx-plane.

During the acceleration phase, ASTER-30 is composed of two parts: the booster and the dart. Both of them can be modeled as cylindrical pipes. The booster section has a diameter of 36 cm and the dart is 18 cm wide. The skin thickness[1] of the missile is 2.5 mm. These dimensions are illustrated in Figure 2.

The material used for the missile is assumed to be 30% carbon fibres composites and unidirectional along the longitudinal axis. The Young modulus along the x-axis is $E = 180\,GPa$ for such a material. The second moment of area at the neutral axis along y-axis for a cylindrical section is:

$$I_{G,y} = \pi \frac{D^4 - (D - 2\,e)^4}{64}$$

with D and e the external diameter and thickness of the pipe. Thus, the second moment of area for the booster and the dart are :

$$\begin{cases} I_{G,y_{booster}} & = 4.49 \cdot 10^{-5}\,m^4 \\ I_{G,y_{dart}} & = 5.49 \cdot 10^{-6}\,m^4 \end{cases}$$

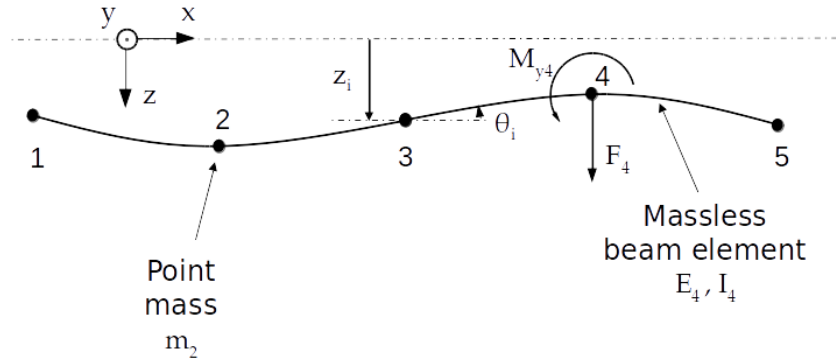[1]Estimated from the natural frequency of the 1st bending mode at 20Hz

Figure 3: Lumped Element Model of a Beam (5 nodes)

It is assumed that the missile mass is equally distributed in the dart and in the booster therefore the linear mass density ρ_m is uniform in the booster, and uniform in the dart:

$$\begin{cases} \rho_{m_{booster}} &= 140.9 \, kg.m^{-1} \\ \rho_{m_{dart}} &= 51.9 \, kg.m - 1 \end{cases}$$

It is necessary to discretize the body in order be able to conduct a state-space representation and simulations. To reach this goal, the mathematical model of the structure is designed using a lumped element model illustrated in Figure 3.

Geometry The missile is longitudinaly discretized in n nodes evenly spaced by the beams length $l = \frac{L}{n-1}$. The nodes i and $i+1$ are linked together by a massless Euler-Bernoulli beam i. Let z_i, $\dot{z}_i$ and $\ddot{z}_i$ be respectively the displacement, speed and acceleration of node i along the z-axis. θ_i, $\dot{\theta}_i$ and $\ddot{\theta}_i$ are respectively the pitch angle, pitch rate and pitch acceleration of the beams at the junction node i.

To determine the number of nodes needed, we can consider looking at the natural frequencies of the beam converging as n grows. On Figure 4, first structural mode frequencies have been computed[2] for n varying between 7 and 300. The frequency converges when n increases. Eventually $n = 100$ is a good choice to minimize the number of nodes for computational efficiency and having an acceptable accuracy on natural frequencies. Indeed, at about $n = 100$, the frequency oscillates between $19.85 \, Hz$ and $20.15 \, Hz$ which corresponds to 1.5% of variation. It is worth noting that the uncertainty on the real first mode frequency is 5 to 10% so with $n = 100$, the first mode frequency can be said as converged.

Mass and stiffness Each node $i \in [\![1, n]\!]$ has a point mass m_i that is the mass of the section from $x = \left(i - \frac{3}{2}\right) l$ to $x = \left(i - \frac{1}{2}\right) l$. Thus the mass is conserved during the

---

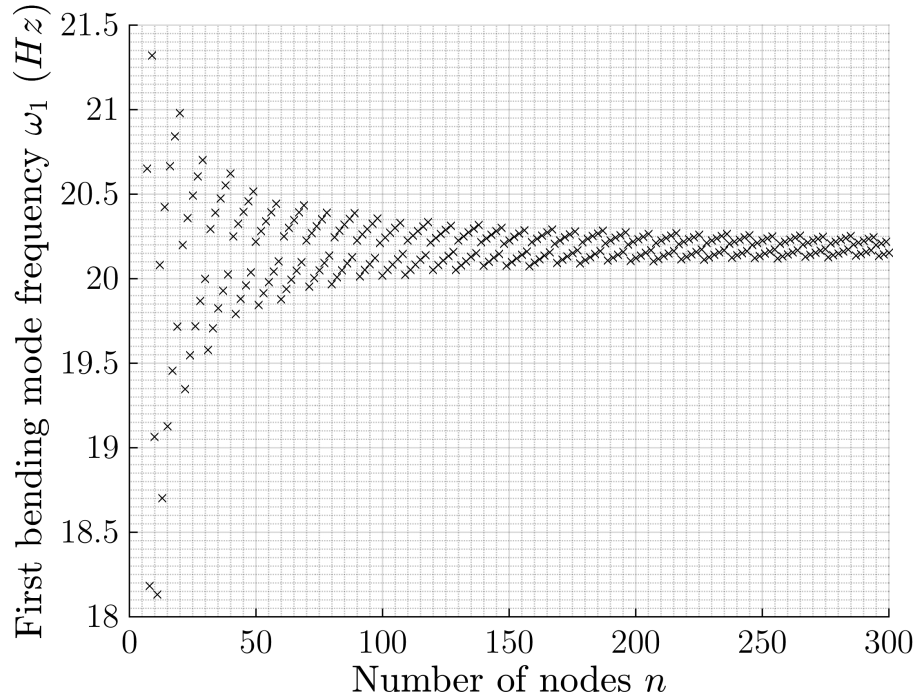[2]The method to do so will be explained later.

Figure 4: Computed First Mode Natural Frequency

discretization : $\sum_{i=1}^{n} m_i = m$. The Euler-Bernoulli beam i has a Young modulus E_i and the second moment of area at neutral axis passing through G and along y-axis $I_{G,y,i}$. For readability purposes, $I_{G,y,i}$ will be noted I_i but the reader must be carefull not to confuse it with a rotational inertia, generally noted J in this paper.

The different structural parameters of the body are summarized in Figure 5 for $n = 100$. It is clear that the booster is stiffer and heavier than the dart.

External efforts   On each node i, an external force F_i along the z-axis and an external moment $M_{y,i}$ along the y-axis are applied.

3.2 Second-Order Structural Model

3.2.1 Nodal Model

To generate a second-order structural model, Prentis and Leckie's method [5] will be used. This finite element model can be fully characterized by the following second-order structural equation:

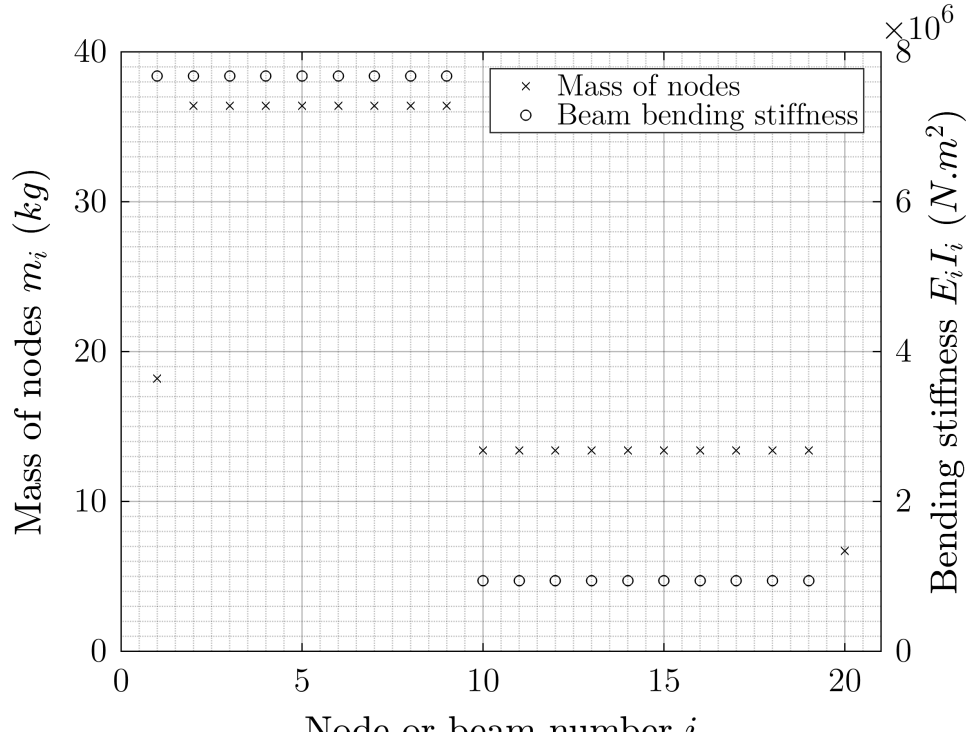$$M' \, \ddot{u} + D' \, \dot{u} + K' \, u = F' \tag{7}$$

Figure 5: Summary of Structural Parameters for 20 Nodes

- $u = \begin{bmatrix} z_1 \\ \vdots \\ z_n \\ \theta_1 \\ \vdots \\ \theta_n \end{bmatrix}$ is the displacement vector

- $F' = \begin{bmatrix} F_1 \\ \vdots \\ F_n \\ M_{y,1} \\ \vdots \\ M_{y,n} \end{bmatrix}$ is the external efforts matrix

- M' is the mass matrix of this system : $M' = \begin{bmatrix} M & 0_{n \times n} \\ 0_{n \times n} & J_y \end{bmatrix}$. M and J_y are diagonal matrices containing nodes masses and rotational inertias about the y-axis.

- K' and D' are the stiffness and damping matrices of this system.

14

K' can be divided in four sub-matrices $K' = \begin{bmatrix} K_{11} & K_{12} \\ K_{21} & K_{22} \end{bmatrix}$. In a static situation where $\ddot{u}$ and $\dot{u}$ are zero, the equation 7 becomes :

$$K'\, u = F' \tag{8}$$

Thus

$$\begin{bmatrix} K_{11} & K_{12} \\ K_{21} & K_{22} \end{bmatrix} \begin{bmatrix} z \\ \theta \end{bmatrix} = \begin{bmatrix} F \\ M_y \end{bmatrix}$$

Finding K' To derive this matrix, one can **consider only two nodes i and $i+1$** linked with the beam i. The equation8 is simplified to:

$$\begin{bmatrix} k_{11,i} & k_{12,i} \\ k_{21,i} & k_{22,i} \end{bmatrix} \begin{bmatrix} z_i \\ z_{i+1} \\ \theta_i \\ \theta_{i+1} \end{bmatrix} = \begin{bmatrix} F_i \\ F_{i+1} \\ M_{y,i} \\ M_{y,i+1} \end{bmatrix}$$

Four cases are considered and illustrated in Figure 6:

	z_i	z_{i+1}	θ_i	θ_{i+1}
Case 1	1	0	0	0
Case 2	0	1	0	0
Case 3	0	0	1	0
Case 4	0	0	0	1

The forces and moments applied to the beam are F_i, F_{i+1}, $M_{y,i}$ and $M_{y,i+1}$. The equilibrium between external efforts on the beam gives the two equations (forces and moments at node i):

$$F_i + F_{i+1} = 0 \tag{9}$$

$$M_{y,i} + M_{y,i+1} - l \cdot F_{i+1} = 0 \tag{10}$$

Using beam theory, the deformation and efforts are linked with the equation

$$E_i\, I_i\, \frac{\partial^2 z}{\partial x^2}(x) = -M_y(x) \tag{11}$$

where and $M_y(x) = M_{y,i+1} - (l - x)\, F_{i+1}$ are local young modulus, second moment of area and pitching moment at abscissa x [3]. For readability purposes, $E_i\, I_i$ will now be noted EI_i. This yields after integration and double integration

$$EI_i \theta(x) = -\frac{1}{2} x^2\, F_{i+1} + x\,(-M_{y,i+1} + l\, F_{i+1}) + A \tag{12}$$
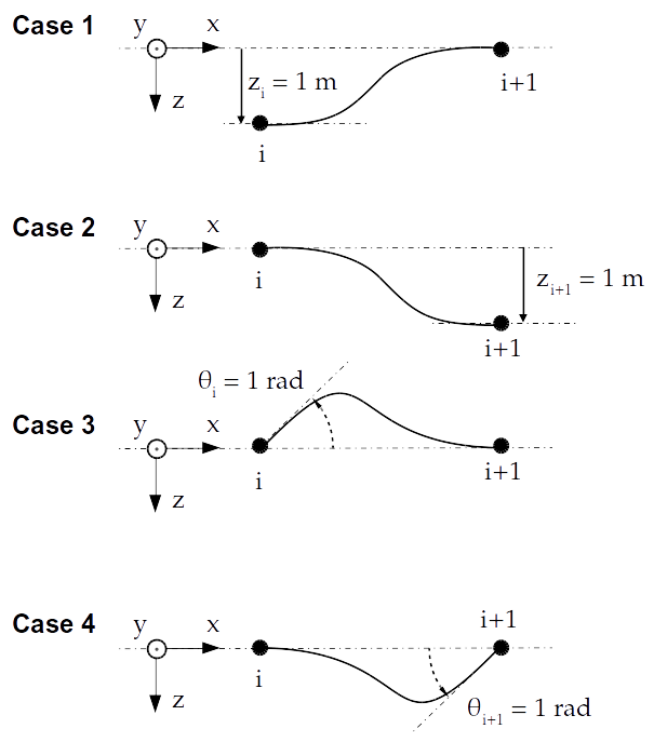
---

[3] $x = 0$ at node i and $x = l$ and node $i+1$

Figure 6: Elementary Cases for Two Nodes

$$EI_i z(x) = -\frac{1}{6}x^3 F_{i+1} + \frac{1}{2}x^2 \left(-M_{y,i+1} + l\, F_{i+1}\right) + A\, x + B \tag{13}$$

with A and B integration constants.

The boundary conditions are

$$\begin{cases} \theta(0) & = \theta_i \\ \theta(l) & = \theta_{i+1} \\ z(0) & = z_i \\ z(l) & = z_i \end{cases} \tag{14}$$

Thus, the system of equations 9, 10, 12, 13 and 14 for each case 1 to 4 yields :

	Case 1	Case 2	Case 3	Case 4
F_i	$12\,EI_i\big/l^3$	$-12\,EI_i\big/l^3$	$-6\,EI_i\big/l^2$	$-6\,EI_i\big/l^2$
F_{i+1}	$-12\,EI_i\big/l^3$	$12\,EI_i\big/l^3$	$6\,EI_i\big/l^2$	$6\,EI_i\big/l^2$
$M_{y,i}$	$-6\,EI_i\big/l^2$	$6\,EI_i\big/l^2$	$4\,EI_i\big/l$	$2\,EI_i\big/l$
$M_{y,i+1}$	$-6\,EI_i\big/l^2$	$6\,EI_i\big/l^2$	$2\,EI_i\big/l$	$4\,EI_i\big/l$

thus $k_{11,i}$, $k_{12,i}$, $k_{21,i}$ and $k_{22,i}$ derived from the table above are

$$\begin{cases} k_{11,i} & = \frac{12\,EI_i}{l^3} \begin{bmatrix} 1 & -1 \\ -1 & 1 \end{bmatrix} \\[2em] k_{12,i} = k_{21,i}^T & = \frac{6\,EI_i}{l^2} \begin{bmatrix} -1 & -1 \\ 1 & 1 \end{bmatrix} \\[2em] k_{22,i} & = \frac{2\,EI_i}{l} \begin{bmatrix} 2 & 1 \\ 1 & 2 \end{bmatrix} \end{cases}$$

Now considering the complete missile, as the element beams are linked in serie, the matrices K_{11}, K_{12}, K_{21}, and K_{22} can be calculated by summing the matrices $k_{11,i}$, $k_{12,i}$, $k_{21,i}$ and $k_{22,i}$ on the diagonal as shown below for K_{11}:

Thus, these matrices are

$$K_{11} = \frac{12}{l^3} \begin{bmatrix} EI_1 & -EI_1 & 0 & \cdots & & 0 \\ -EI_1 & EI_1 + EI_2 & \ddots & & \ddots & \vdots \\ 0 & \ddots & \ddots & & \ddots & 0 \\ \vdots & & \ddots & \ddots & EI_{n-2} + EI_{n-1} & -EI_{n-1} \\ 0 & \cdots & & 0 & -EI_{n-1} & EI_{n-1} \end{bmatrix}$$

$$K_{12} = K_{21}^T = \frac{6}{l^2} \begin{bmatrix} -EI_1 & -EI_1 & 0 & \cdots & & 0 \\ EI_1 & EI_1 - EI_2 & \ddots & & \ddots & \vdots \\ 0 & \ddots & \ddots & & \ddots & 0 \\ \vdots & & \ddots & \ddots & EI_{n-2} - EI_{n-1} & -EI_{n-1} \\ 0 & \cdots & & 0 & EI_{n-1} & EI_{n-1} \end{bmatrix}$$

$$K_{22} = \frac{2}{l} \begin{bmatrix} 2\,EI_1 & EI_1 & 0 & \cdots & & 0 \\ EI_1 & 2\,EI_1 + 2\,EI_2 & \ddots & & \ddots & \vdots \\ 0 & \ddots & \ddots & & \ddots & 0 \\ \vdots & & \ddots & \ddots & 2\,EI_{n-2} + 2\,EI_{n-1} & EI_{n-1} \\ 0 & \cdots & & 0 & EI_{n-1} & 2\,EI_{n-1} \end{bmatrix}$$

It is worth noting that $K' = K'^T$ that can be explained by Maxwell-Betti reciprocal work theorem.

Simplified second-order structural model In this study, we assume that the pure external moments $M_{y,i}$ are negligeable when compared to moments created by the forces F_i. The missile is modeled as an Euler-Bernoulli beam, thus the local rotational inertias I_i are zero. The damping D' is very few for such flexible structures so it can be neglected for the next trick. With these hypotheses, the lower part of Equation 7 concerning rotational acceleration becomes :

$$0_{n \times 1}\,\ddot{\theta} + 0_{n \times 1}\dot{\theta} + K_{21}z + K_{22}\theta = 0_{n \times 1}$$

K_{22} is a symmetric tridiagonal matrix which invertibility can be proven by LU decomposition[1]. This leads to the important relation between z and θ:

$$\theta = -K_{22}^{-1}\,K_{21}z \tag{15}$$

This equation mean that the second part of u can be entirely determined from its first part. The upper part of the Equation 7 fully describes the structural system:

$$M\,\ddot{z} + D\,\dot{z} + (K_{11} - K_{12}K_{22}^{-1}K_{21})\,z = F$$

The stiffness matrix is then $K = K_{11} - K_{12}K_{22}^{-1}K_{21}$. One can verify that $K^T = K$.

The damping matrix is chosen proportionnal to K and set to damp the first structural mode to 1%. This gives $D = K/6000$. The second-order structural equation is as follows:

$$M \ddot{z} + D \dot{z} + K z = F \tag{16}$$

3.2.2 Modal Model

The triplet (M,D,K) is the nodal realization of the second-order structural model. A modal realization must be found to extract the flexible body modes from the structural model. The transformation of the nodal model is described in [3] and can be derived as follows.

Considering free vibrations without damping, the system being linear, the displacement vector will be $z = \phi e^{j\omega t}$ with ϕ constant thus $\ddot{z} = -\omega^2 \phi e^{j\omega t}$ and Equation 16 becomes:

$$\left(-\omega^2 M + K\right) \phi = 0 \tag{17}$$

Non-trivial solutions to Equation 17 (i.e. $\phi \neq 0$) exist if and only if

$$\det(-\omega^2 M + K) = 0$$

The solutions are the generalized eigen values $(\omega_1^2, \omega_2^2, ..., \omega_n^2)$ of the matrices K and M. $(\omega_1, \omega_2, ..., \omega_n)$ are the natural frequencies of the structure and the eigen vectors $(\phi_1, \phi_2, ..., \phi_n)$ are the natural modes also called modes shape.

In this particular study, the structure extremities are free hence the two first natural frequencies are $0\,Hz$ and the two first natural modes correspond to the rigid-body modes: z-axis translation and y-axis rotation. The natural frequencies and modes shape are renamed $(0, 0, \omega_1, \omega_2, ..., \omega_{n-2})$ and $(\phi_{0,1}, \phi_{0,2}, \phi_1, \phi_2, ..., \phi_{n-2})$.

The modes shape of the rigid-body and the first three bending modes are plotted in Figure 7. This figure shows that the dart is likely to bend more than the booster. Indeed, the front part of the missile is more flexible so it will bend more.

The natural frequencies for the first modes are summarized in Table 1.

Let $\Phi = [\phi_{0,1}\ \phi_{0,2}\ \phi_1\ \phi_2\ ...\ \phi_{n-2}]$ be the modal matrix and

$$\Omega = \begin{bmatrix} 0 & & & & & \\ & 0 & & & & \\ & & \omega_1 & & & \text{\Large 0} \\ & & & \ddots & & \\ \text{\Large 0} & & & & \omega_{n-2} \end{bmatrix}$$

be the matrix of natural frequencies.

Let z_m be the displacement vector of modes defined by $z = \Phi z_m$. The modal matrices of mass M_m, damping D_m and stiffness K_m are obtained as follows
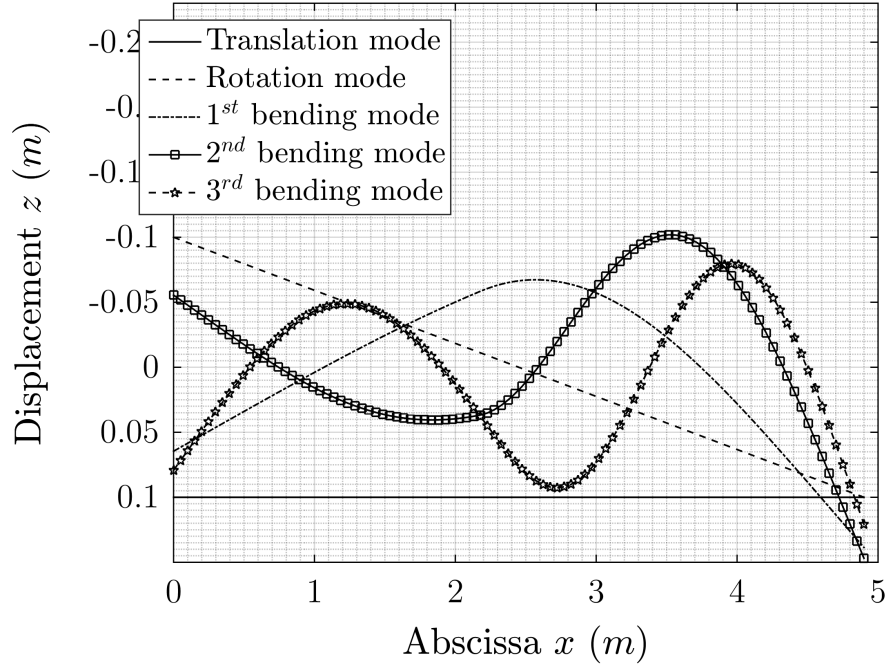
Figure 7: Modes Shape of ASTER-30

| Mode | Natural Frequency | | Damping Ratio |
	(Hz)	$(rad.s^{-1})$	
z translation mode	0	0	0
y rotation mode	0	0	0
1st bending mode	20.0	125	1.0%
2nd bending mode	67.7	425	3.5%
3rd bending mode	139.7	877	7.3%
4th bending mode	213.9	1344	11%
5th bending mode	335.1	2106	17%

Table 1: Natural Frequencies and Damping Ratios of Modes

$$M_m = \Phi^T M \Phi$$

$$D_m = \Phi^T D \Phi$$

$$K_m = \Phi^T K \Phi$$

The triplet (M_m, D_m, K_m) defines the second-order structural modal model of the missile. The equation 16 becomes:

$$M_m \, \ddot{z}_m + D_m \, \dot{z}_m + K_m \, z_m = \Phi^T F \tag{18}$$

3.2.3   Output equation

Three types of sensors are investigated in this paper to measure vibrations: strain gages, gyrometers and accelerometers. Their measurement can be represented by the output equation:

$$y = C_{oz}z + C_{ov}\dot{z} + D_oF \tag{19}$$

where y is a vector containing the measurement of all sensors.

It means that the signal measured by the sensors are a linear combination of the displacement of the nodes (matrix C_{oz}), their speed (matrix C_{ov}) and also a feedforward term D_o on the external forces applied on the nodes.

Gyrometer   A gyrometer on node i measures $\dot{\theta}_i$, thus n gyrometers can be placed. Since q is often used to represent the pitch rate, this letter will be used for gyrometer output matrices. According to Equation 15, $\theta = -K_{22}^{-1}K_{21}z$, therefore $\dot{\theta}_i = -K_{22}^{-1}K_{21}\dot{z}$. This yields the output matrices

$$C_{ozq} = 0_{n\times n} \qquad C_{ovq} = -K_{22}^{-1}K_{21} \qquad \text{and} \qquad D_{oq} = 0_{n\times n}$$

Accelerometer   An accelerometer on node i measures $\ddot{z}_i$. The letter assigned to acceleration measurement will be a like "acceleration" and the measurement will be called a_z. With an accelerometer on each node, there are n accelerometers. In Equation 19, $\ddot{z}$ does not appear. But using the second-order structural equation 16:

$$\ddot{z} = -M^{-1}K \, z - M^{-1}D \, \dot{z} + F$$

thus

$$C_{oza} = -M^{-1}K \qquad C_{ova} = -M^{-1}D \qquad \text{and} \qquad D_{oa} = Id_n$$

Strain gage For a strain gage, a first order Taylor developpement to approximate the spatial derivative of $\theta(x)$ at node i will be conducted. This approximation cannot be made on nodes 1 and n therefore, only $n - 2$ strain gages are considered. The letter used for this sensor is ε which is often assigned to strains.

The Euler-Bernoulli beam theory assumes that each section stays perpendicular to the neutral axis. The strain gages are placed on the upper side of the missile therefore, the local deformation at the surface is

$$\varepsilon(x) = -\frac{\partial \theta}{\partial x} \frac{D(x)}{2}$$

where $D(x)$ is the local missile diameter. It is worth noting that $\varepsilon(x)$ is positive when the strain gage is stretched and negative when it is compressed.

The partial derivative of θ with respect to x is approximated using a first order Taylor developpement at node $i \in [\![2, n-1]\!]$:

$$\frac{\partial \theta}{\partial x}(x_i) \simeq \frac{\theta_{i+1} - \theta_{i-1}}{2\,l}$$

thus

$$\varepsilon_i = \frac{-\theta_{i+1} + \theta_{i-1}}{2\,l} \frac{D_i}{2}$$

Let $\varepsilon = (\varepsilon_i)_{i \in [\![2, n-1]\!]}$, then the previous equation yields

$$\varepsilon = T_\varepsilon \theta$$

with

$$T_\varepsilon = \frac{1}{4\,l} \begin{bmatrix} D_2 & 0 & -D_2 & & & & & \text{\Large 0} \\ & D_3 & 0 & -D_3 & & & & \\ & & D_4 & 0 & -D_4 & & & \\ & & & \ddots & \ddots & \ddots & & \\ & & & & D_{n-2} & 0 & -D_{n-2} & \\ \text{\Large 0} & & & & & D_{n-1} & 0 & -D_{n-1} \end{bmatrix}$$

Finally, using Equation 15, the relation becomes

$$\varepsilon = -T_\varepsilon K_{22}^{-1} K_{21} z$$

hence

$$C_{oz\varepsilon} = -T_\varepsilon K_{22}^{-1} K_{21} \qquad C_{ov\varepsilon} = 0_{(n-2) \times n} \qquad \text{and} \qquad D_{o\varepsilon} = 0_{(n-2) \times n}$$

Concatenation   The output vector corresponding to the concatenation of all mea-

surements is $y = \begin{bmatrix} \varepsilon \\ q \\ a_z \end{bmatrix}$ .Therefore

$$C_{oz} = \begin{bmatrix} C_{oz\varepsilon} \\ C_{ozq} \\ C_{oza} \end{bmatrix} \qquad C_{ov} = \begin{bmatrix} C_{ov\varepsilon} \\ C_{ovq} \\ C_{ova} \end{bmatrix} \qquad \text{and} \qquad D_o = \begin{bmatrix} D_{o\varepsilon} \\ D_{oq} \\ D_{oa} \end{bmatrix}$$

Modal output matrix   The Output Equation 19 will finally be

$$y = C_{oz}\Phi z_m + C_{ov}\Phi \dot{z}_m + D_o F$$

defining the modal equivalent of the output matrices :

$$y = C_{mz}z_m + C_{mv}\Phi \dot{z}_m + D_o F$$

with

$$\begin{cases} C_{mz} &= C_{oz}\Phi \\ C_{mv} &= C_{ov}\Phi \end{cases}$$

3.3   Rigid-body Modes Elimination

The second-order structural model and its output equation in there modal forms have been derived. However, the two rigid-body modes - translation and rotation - must be eliminated. Indeed, this Chapter aims at modeling only vibrations during the flight. The rigid-body dynamics modeled have been derived isolated from gravity and air and do not reflect flight dynamics hence they must be suppressed to keep only vibrations dynamics.

The matrices M_m, D_m and K_m are diagonal meaning that there is no interaction between modes in Equation 18. The rigid-body modes are eliminated by erasing the two first rows of Φ. Hence it is now $\Phi = [\phi_1 \, \phi_2 \, \ldots \, \phi_{n-2}]$ and z_m only contains structural modes displacement. By doing so, modal mass, damping and stiffness matrices size is now $(n-2) \times (n-2)$.

Looking at the output Equation 19, truncating the rigid-body modes will remove rigid-body pitch rate and strain measurement is not influenced by rigid-body modes. However, great care must be taken for the acceleration measurement as $D_{oa} \neq 0$. To compute the acceleration measurements only due to the vibrations, the acceleration measurements due to the rigid-body modes will be calculated considering a rigid structure.

If the missile is considered as a solid, the equation of lateral acceleration at the center of gravity is:

$$a_{z,CG} = \frac{1}{m}F_z$$

and the equation of rotational acceleration is

$$\ddot{\theta} = \frac{1}{J_{y,CG}} M_{y,CG}$$

where F_z is the sum of external forces along the z-axis, $M_{y,CG}$ is the sum of moments applied at the center of gravity along the y-axis, m and J_y are the mass and rotational inertia about the center of gravity along the y-axis. The force and moments are:

$$F_z = \sum_{j=1}^{n} F_j$$

$$M_{y,CG} = \sum_{j=1}^{n} (x_{CG} - x_j) F_j$$

The acceleration at each node i is

$$a_{z,i} = a_{z,CG} + (x_{CG} - x_i) \ddot{\theta}$$

Hence, it yields

$$a_{z,i} = \frac{1}{m} \sum_{j=1}^{n} F_j + (x_{CG} - x_i) \frac{1}{J_y} \sum_{j=1}^{n} (x_{CG} - x_j) F_j$$

In matrix formulation,

$$a_{z,rb} = D_{oa,rb} F$$

where

$$D_{oa,rb} = \frac{1}{m} I d_n + \frac{1}{J_y} \begin{bmatrix} x_{CG} \\ x_{CG} - l \\ \vdots \\ x_{CG} - (n-2)l \\ x_{CG} - (n-1)l \end{bmatrix} \begin{bmatrix} x_{CG} & x_{CG} - l & \cdots & x_{CG} - (n-2)l & x_{CG} - (n-1)l \end{bmatrix}$$

Finally, the output matrix $D_{oa,rb}$ is subtracted from D_{oa} to obtain the output matrix from vibrations only :

$$D_{oa,fb} = D_{oa} - D_{oa,rb}$$

However, this is not completely correct. Indeed, the rigid-body dynamics are different when the missile is considered as flexible. Therefore the rigid-body component in D_{oa} is not $D_{oa,rb}$. Looking at the Bode plot of the transfer function[4] from F_1 to

---

[4]Established later

$a_{z,75}$ on Figure 8, with this first rigid-body substraction technique, at $\omega = 0$, $a_{z,75}(\omega)$ is not zero (curve "a_z,fb imperfect). This is incorrect because at $\omega = 0$, the vibrations are not excited then they should be inexistant and $a_{z,75} = 0$. Once the state space representation will be established, the good correction will be applied.

3.4   State Space Model

Previously, the second-order structural model in its modal form without the rigid-body modes has been derived. This representation is not convenient for control design. Therefore a state-space representation of this system will be created.

3.4.1   From Second-Order Model to State Space Model

The system must firstly be translated into a state space representation.

Now that the rigid-body modes are eliminated, K_m is positive-definite and we can define

$$\Omega = M_m^{-1/2} K_m^{1/2}$$

$$Z = \frac{1}{2} M_m^{-1} D_m \Omega^{-1}$$

Z is a diagonal matrix containing the modes damping ratios. For instant $Z_{3,3} = \zeta_3$ is the damping ratio of the third bending mode.

The state vector is defined as $x = \begin{bmatrix} z_m \\ \dot{z}_m \end{bmatrix}$. The input vector is $u = F$. The ouput vector is $y = \begin{bmatrix} \varepsilon \\ q \\ a_z \end{bmatrix}$ Thus
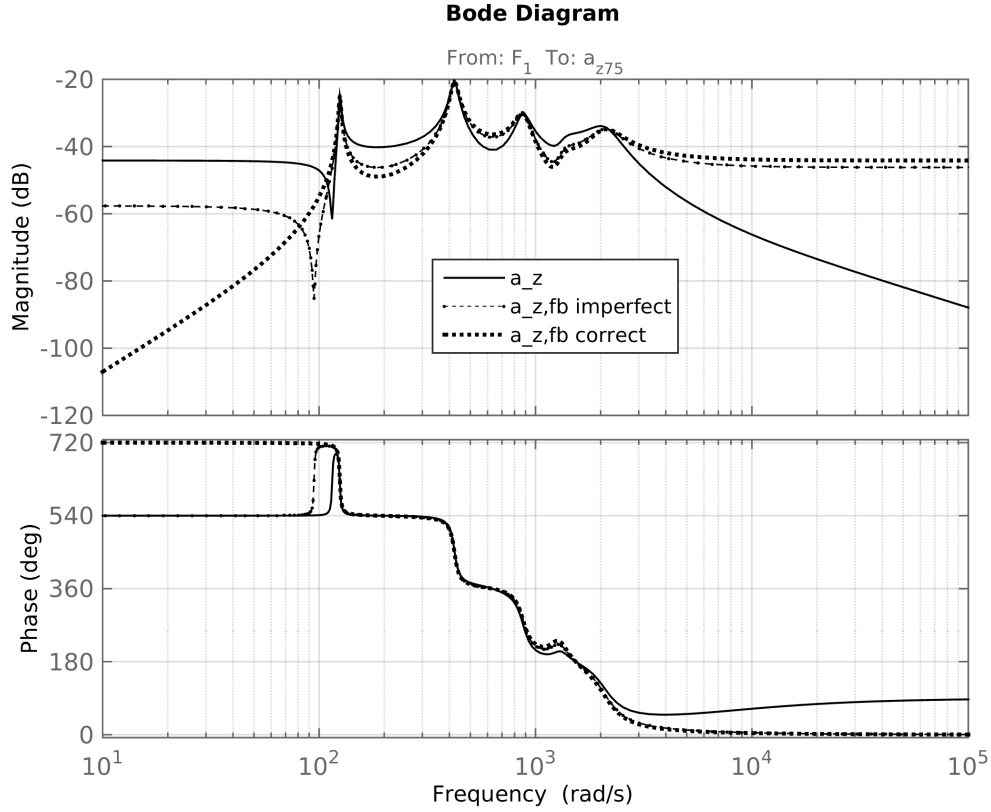
$$\dot{x} = A\,x + B\,u$$

$$y = C\,x + D\,u$$

with

$$A = \begin{bmatrix} 0_{(n-2)\times(n-2)} & Id_{n-2} \\ -\Omega^2 & -2Z\Omega \end{bmatrix}$$

$$B = \begin{bmatrix} 0_{(n-2)\times n} \\ \Phi^T \end{bmatrix}$$

$$C = \begin{bmatrix} C_{mz} & C_{mv} \end{bmatrix}$$

$$D = D_o = \begin{bmatrix} 0_{(n-2)\times n} \\ 0_{n\times n} \\ D_{oa,fb} \end{bmatrix}$$

Figure 8: Bode plot of F_1 to $a_{z,75}$

In the previous part, $D_{oa,fb}$ has not been clearly defined. To eliminate properly rigid-body dynamics measured by acceleration sensors, the following technique can be used. The acceleration due to rigid-body dynamics is composed of a feedforward term $D_{oa,rb}$ only. In the transfer function, this is a static gain. Thus, one can just remove this static value :

$$a_z(j\omega) = -C_{ma}(A - j\omega\,Id)^{-1}B + D_{oa,fb}$$

where $C_{ma} = \begin{bmatrix} C_{mza} & C_{mva} \end{bmatrix}$. At $\omega = 0$, $a_z = 0$ so $D_{oa,fb} = C_{ma}A^{-1}B$.

Thanks to this, a_z is 0 at low frequency as shown in Figure 8 (curve "a_z,fb correct").

3.4.2   Formulation in State Space Modal Form 2

Gawronski [3] gives a convenient state space formulation of the structural system. It is the modal form 2. In this form, the state vector is

26

$$x_m = \begin{bmatrix} z_{m,1} \\ z_{mo,1} \\ z_{m,2} \\ z_{mo,2} \\ \vdots \\ z_{m,(n-2)} \\ z_{mo,(n-2)} \end{bmatrix}$$

where $z_{mo,i} = \zeta_i z_{m,i} + \dot{z}_{m,i}/\omega_i$. In this form, the modal state matrix A_m has the particular form:

$$A_m = \begin{bmatrix} A_{m1} & & & \\ & A_{m2} & & \\ & & \ddots & \\ & & & A_{m(n-2)} \end{bmatrix}$$

with $A_m = \begin{bmatrix} -\zeta_i\omega_i & \omega_i \\ \omega_i & -\zeta_i\omega_i \end{bmatrix}$.

The transformation matrix V_m defined as $x = V_m x_m$ for 4 modes is

$$V_m = \begin{bmatrix} 1 & 0 & & & & & & \\ & & 1 & 0 & & & & \\ & & & & 1 & 0 & & \\ & & & & & & 1 & 0 \\ -\omega_1/\zeta_1 & \omega_1 & & & & & & \\ & & -\omega_2/\zeta_2 & \omega_2 & & & & \\ & & & & -\omega_3/\zeta_3 & \omega_3 & & \\ & & & & & & -\omega_4/\zeta_4 & \omega_4 \end{bmatrix}$$

Hence, $B_m = BV_m$, $C_m = CV_m$ and $D_m = D$.

This final state-space realization (A_m, B_m, C_m, D_m) is the modal state-space model of the vibrations of the missile with outputs y containing $n - 2$ strain measurements ε_i, n gyrometer measurements q_i and n accelerometers a_{zi}. This vibrations model will then be added to the flight dynamics model.

3.5   Model Reduction

Currently, the structural model has $n - 2$ bending modes. The number of nodes chosen is 100 so 98 modes are considered. Most of the high frequency modes are inaccurate because of the Euler-Bernoulli model which is suitable for low frequency dynamics. Fortunately, these modes do not contribute much to the system dynamics. A way to compare every mode contribution is to use the Hankel singular values decomposition of the system. On Figures 9, 10, 11, the state contribution in the Hankel singular values have been plotted for the three different types of sensor. The state vector is
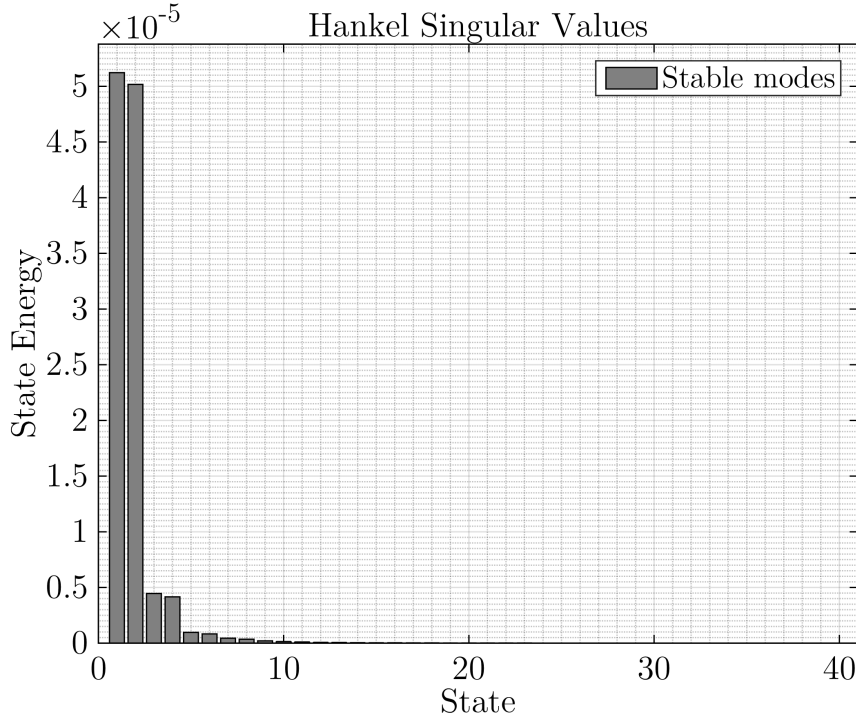
Figure 9: Hankel Singular Values Decomposition - Strain Gages Output

$x_m = \begin{bmatrix} q_{mi} \\ q_{moi} \end{bmatrix}_i$. The first five bending modes will be kept, the others are truncated. Indeed, on these bar plots, the contribution of the 6th bending mode (bar 10 and 11) and higher (12 and above) is negligible. These modes correspond to less than 0.5% of the singular value of the 1st mode for the strain gages, less than 1% for the gyrometers and 5% for the accelerometers.

To reduce the model to the five first modes, the new state space model is $(A_m^5, B_m^5, C_m^5, D_m^5)$. A_m^5 is the 10×10 upper left corner of A_m, B_m^5 is the 10 first rows of B_m, C_m^5 is the 10 first columns of C_m and D_m^5 is equal to D_m.

From now on, $(A_m^5, B_m^5, C_m^5, D_m^5)$ will be simply named (A, B, C, D).

4   Actuator & Sensor Placement

4.1   Actuator Placement

The goal of this paper is to enhance the global performance of ASTER-30 by adding sensors. No actuators from the original model will be added hence the only actuators available are the thrust vectoring by nozzle orientation at the very rear of the missile and the fins at the tail of the dart. The position of these two actuators on the airframe are $x_{nozzle} = 0\,m$ and $x_{fins} = 2.4\,m$. These positions corresponds to the nodes 1 and
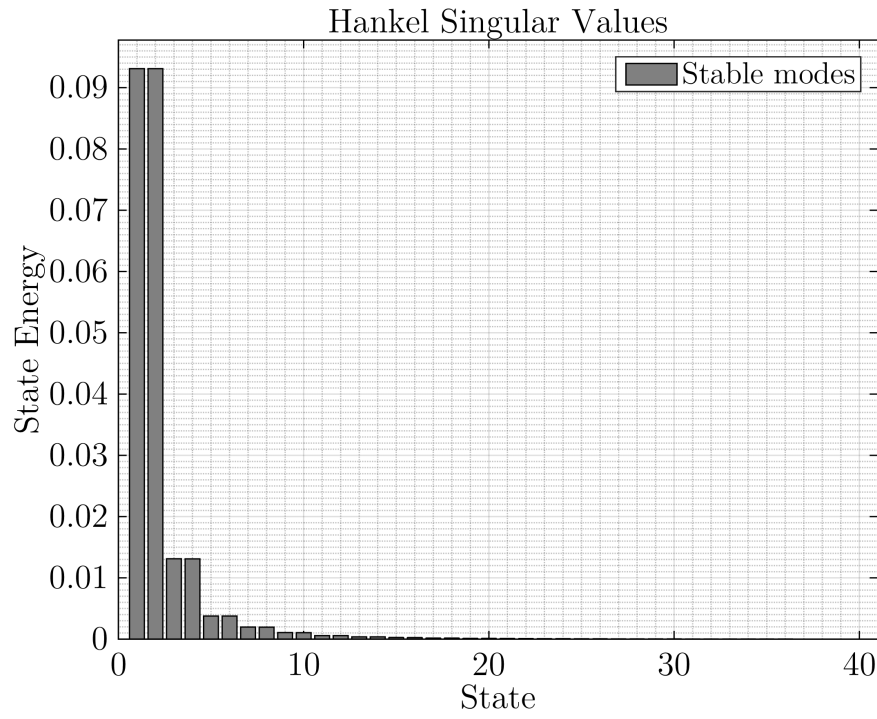
Figure 10: Hankel Singular Values Decomposition - Gyrometers Output
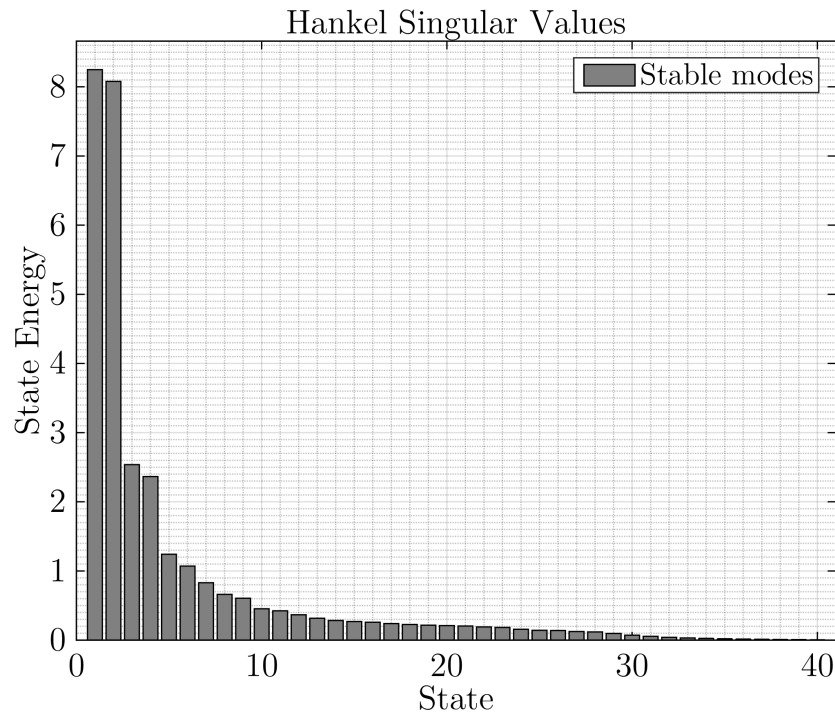

Figure 11: Hankel Singular Values Decomposition - Accelerometers Output

50.

It is assumed that the vibrations are mainly excited by the lateral forces generated by these two actuators. The aerodynamic forces are too distributed and weak compared to the rocket motor lateral thrust at the rear of the booster.

The only inputs to the vibration system are thus lateral forces at nodes 1 and 50. The previous system (A,B,C,D) is modified[5] to keep only the inputs F_1 and F_{50}.

4.2 Sensor Placement

The state space model developed in the previous section outputs three different types of sensors : strain gages, gyrometers and accelerometers on all possible node[6]. However, only some of these sensors need to be kept. For each of these types of sensor, the minimum number required to control the structure will be computed and the optimal locations will be determined using a technique of placement.

4.2.1 Placement Indices

Gawronski gives a method to quantitatively assess the location of a sensor given its type [3]. He proposes three different norms : the H_2 Norm, the H_∞ Norm and the Hankel Norm. Here, the placement will rely on H_∞ Norm. The sensors will be placed only considering the 1st bending mode. The higher modes have high natural frequencies that cannot be actively damped. Indeed Table 1 gives natural frequencies for the 2nd mode and higher above 25Hz which is the cutoff frequency of the actuators.

The first step is to select a set of possible locations for a type of sensor. Let be $S = \{i_1, i_2, \ldots, i_s\}$ this set with s the number of possible locations. At each of these locations, an index is calculated which represents the ability of the sensor to sense the 1st bending mode at this place. This index is called σ_i for the node i. A simple way to define it is

$$\sigma_i = \|G_{1i}\|_\infty$$

where G_{1i} is the transfer function of $[F_1, F_{50}]$ to the sensor considered at node i considering only the 1st mode.

The damping ratio of the 1st bending mode is only 1% so the following approximation can be made:

$$G_{1i} \simeq \frac{\|B_1\|_2 \|C_{i1}\|_2}{2\zeta_1\omega_1}$$

The matrices B_1 and C_{i1} are the input and output matrices at node i for the sensor considered and the 1st bending mode. B_1 is the first two rows of B and C_{i1} is the first two columns of the part of C corresponding to the type of sensor considered.

---

[5] Only columns 1 and 50 of B and D are kept

[6] $n - 2$ for the strain gages and n for the gyrometers and the accelerometers

The bigger is σ_i the greater is the amplitude of the signal measured by the sensor at node i. Thanks to this method, the locations can be ranked to determine the optimal position to place the sensors. For each type of sensor - strain gages, gyrometers and accelerometers - this technique will be used.

4.2.2   Strain Gages Placement

A strain gage is a long resistor fixed on the skin of the structure. When the skin is stretched or compressed, the strain gage is deformed and the electrical resistance changes. These variations of electrical resistance can be precisely measured with a Weathstone bridge. The great advantage of this sensor is its insensitivity to the rigid-body dynamics of the system. This kind of sensor measures only deformation. Thus, only one of these sensors well placed can determine the flexure of the missile. However, it will be shown later that the signal of this sensor needs to be derivated to damp the 1st mode bending. This derivation is likely to increase noise propagation. Another disadvantage is its great sensitivity to temperature variation. The booster part of the missile is greatly heated by the rocket engine and the head of the dart is aerodynamically heated. The possible locations are $x \in [2.2m,\ 4.4m]$ that corresponds to the set $S = [\![46, 89]\!]$.

The placement indices have been computed at all locations $i \in [\![2, n-1]\!]$ even if the set of location is $S = [\![46, 89]\!]$ to show entirely how these indices vary. They appear on Figure 12.

On the bar plot, the placement indices of locations on the booster are very low compared to those on the dart. Indeed the booster is very stiff so it bends very few compared to the dart. The best location for a strain gage is at node 49 next to the fins at $x = 2.38\,m$. This location corresponds to the strain antinode of the 1st bending mode where the flexure is maximum.

4.2.3   Gyrometers Placement

A gyrometer will measure not only the pitch rate due to the vibrations but also the pitch rate of the rigid-body. For instant, at node i, a gyrometer will measure

$$q_i = q_{i,fb} + q$$

The isolate the pitch rate of the vibrations, one needs the measurements of two gyrometers placed at different locations. Hence, the pitch rate of the rigid-body can be removed by substraction to keep only the vibrations measurement:

$$q_i - q_j = q_{i,fb} - q_{j,fb}$$

At least two gyrometers must be used.

A gyrometer is less sensitive to variations of temperature than a strain gage and can be placed on the booster. However a margin is kept with the two extremities of the missile because the tail is probably dense in technology because of the nozzle and
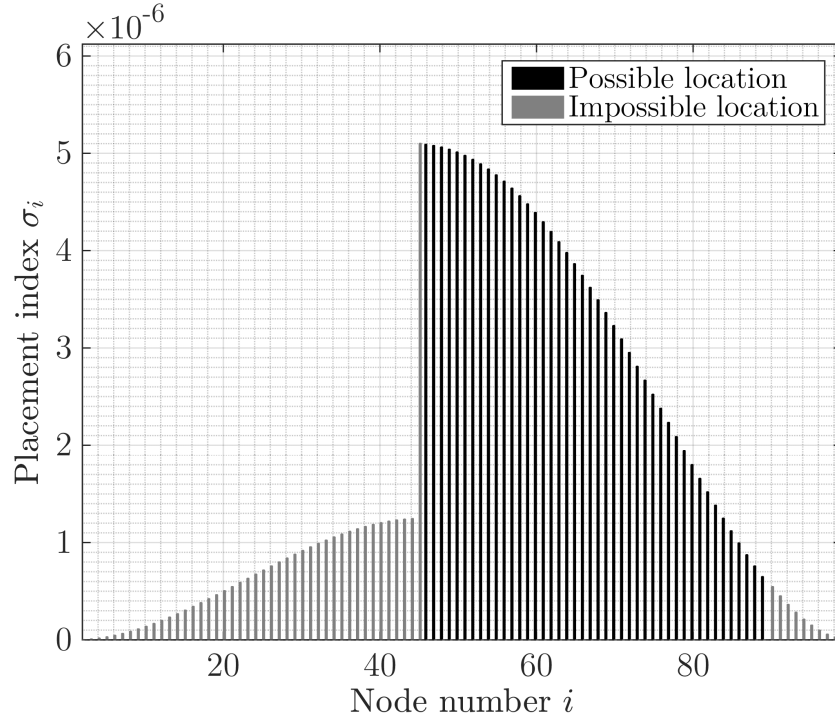
Figure 12: Placement Indices - Strain Gages

the nose contains a radar. For the gyrometers, the set of locations available is then $S = [\![10, 92]\!]$ corresponding to $x = [\![0.45m, 4.40m]\!]$.

Figure 13 shows the placement indices for gyrometers.

The nose is a place where the gyrometer would be very sensitive to the 1st bending mode. Actually, there is already a gyrometer in the sensor pack at x somewhere between $3.9\,m$ and $4.3\,m$ that correspond approximately to node 83. The second gyrometer must be place at the other side of the zero pitch rate node 54. The second best position is then node 10.

4.2.4 Accelerometers Placement

Accelerometers measure the lateral acceleration due to vibrations but also the lateral acceleration of the rigid-body. Moreover, the acceleration on the rigid-body depends of where the sensor is placed. At node i, and accelerometer will measure:

$$a_{z,i} = a_{z,rb,CG} + (x_{CG} - x_i)\,\dot{q} + a_{z,fb,i}$$

thus such a measurement contains three unknowns : $a_{z,rb,CG}$, $\dot{q}$ and $a_{z,fb,i}$. Therefore a minimum number of three accelerometers are needed at different locations to eliminate the acceleration of the center of gravity and the additional term due to pitch acceleration. This also assumes that the position of the center of gravity is accurately known, which is not correct since its position is moving during the propellant combustion.
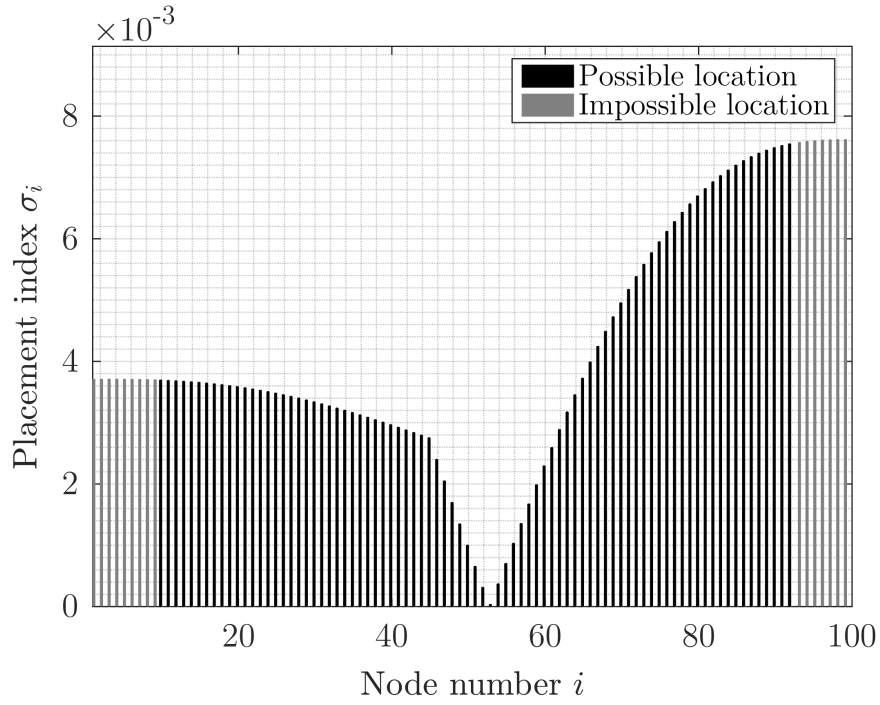
Figure 13: Placements Indices - Gyrometers

Like a gyrometer, an accelerometer is not as sensible to temperature variations as a strain gage. Thus it can be placed within $x = [\![0.45m,\ 4.40m]\!]$ corresponding to the set $S = [\![10, 92]\!]$. Once again, the placement indices are calculated all over the body in Figure 14.

The sensor pack of the missile already contains an accelerometer along the z-axis at node 83. This position is not very sensible to the first bending mode lateral accelerations as its placement index is very low. The sensor pack seems to be placed somewhere next to the vibration acceleration node. Hence this accelerometer cannot be used for bending vibration control.

The three best locations that have a great placement index and are uncorrelated are at nodes 10, 54 and 92.

4.2.5   Outputs Selection

Finally, from the model established in the previous Section, only a few outputs are kept. These outputs are:

- The gyrometer and the accelerometer from the sensor pack at node 83

- The added strain gage at node 49
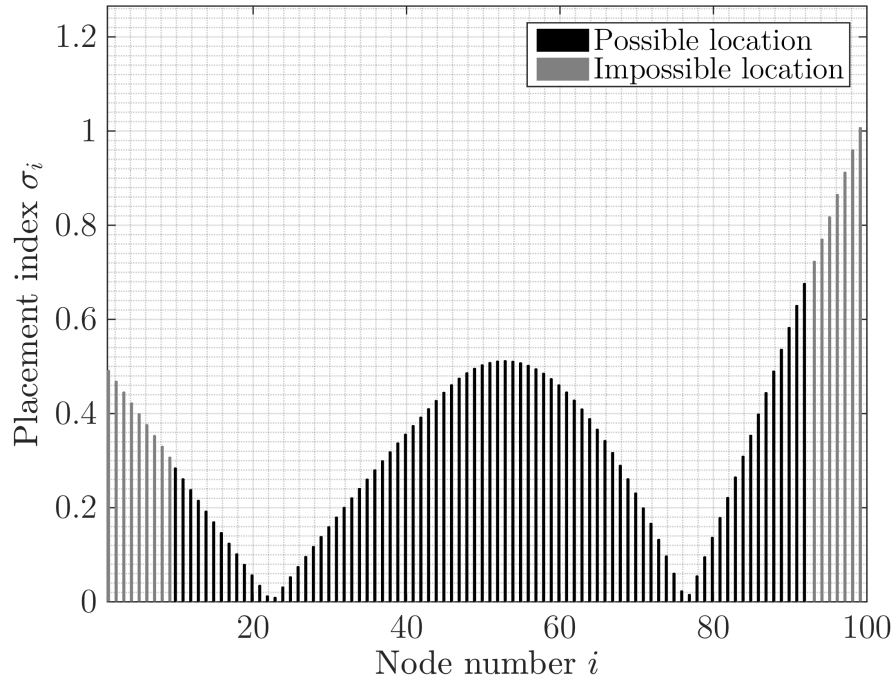
- The added gyrometer at node 10

33

Figure 14: Placement Indices - Accelerometers

- The added accelerometers at nodes 10, 54 and 92

The pitch rate and acceleration outputs at node 83 will be added to the flight dynamics pitch rate and acceleration to simulate the noise created by vibrations in the inertial unit of the missile. The added strain gage at node 49, the gyrometers at nodes 10 and 83 and the three added accelerometers at nodes 10, 54 and 92 will be used to damp the first bending mode.

All of these sensors are summarized in Figure 15.

Part II
Control

References

[1] Moawwad El-Mikkawy and El-Desouky Rahmo. A new recursive algorithm for inverting general tridiagonal and anti-tridiagonal matrices. *Applied Mathematics and Computation*, 204(1):368–372, 2008.

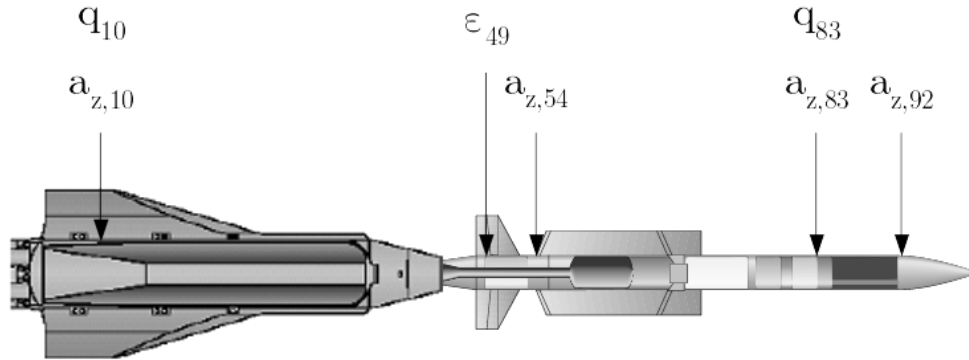[2] Eugene L Fleeman. *Tactical missile design*. Amer Inst of Aeronautics &, 2006.

Figure 15: Sensors Locations - Strain gages ε, Gyrometers q and Accelerometers a_z

[3] Wodek K Gawronski. *Dynamics and control of structures: A modal approach.* Springer Science & Business Media, 2004.

[4] D Lesieutre, J Love, M Dillenius, and AB Blair Jr. Recent applications and improvements to the engineering-level aerodynamic prediction software misl3. In *Proceedings of the 40th AIAA Aerospace Sciences Meeting and Exhibit*, pages 2002–0275, 2002.

[5] James Martin Prentis and Frederick A Leckie. *Mechanical vibrations: an introduction to matrix methods.* Longmans, 1963.